Tellus (1998), 50A, 348–367
Printed in UK – all rights reserved

TELLUS
ISSN 0280–6495

ECBILT: a dynamic alternative to mixed boundary conditions in ocean models

By J. D. OPSTEEGH*, R. J. HAARSMA, F. M. SELTEN and A. KATTENBERG, *KNMI, De Bilt, The Netherlands*

(Manuscript received 7 July 1997; in final form 16 January 1998)

ABSTRACT

As an alternative to the frequently used mixed boundary conditions in ocean GCM's, we present a dynamic atmospheric model (ECBILT) that is simple and yet describes the relevant dynamic and thermodynamic feedback processes to the ocean. This provides the possibility of studying atmosphere/ocean dynamics on very long time-scales of the order of a thousand years. The model is two orders of magnitude faster than AGCMs. We have been running ECBILT with prescribed SSTs for a period of 500 years with seasonal cycle included both in the solar forcing and in the climatological SSTs. The mean state and the variability properties of ECBILT are reasonably realistic. The simulation of the surface fluxes is quite realistic and justifies coupling ECBILT to an ocean GCM. We have done two SST anomaly experiments, one with a tropical SST anomaly as observed during January 1983 and one with an SST anomaly in the northern extra-tropical Atlantic ocean. For the tropical SST anomaly experiment the amount of anomalous precipitation agrees well with what has been found with atmospheric GCM's, but the resulting extra-tropical teleconnection pattern is very weak. The atmospheric response pattern to extra-tropical SST anomalies agrees well with similar SST anomaly experiments performed with atmospheric GCM's. We have tested the performance of ECBILT in coupled mode by coupling it to a simple ocean GCM and thermodynamic sea-ice model and integrating the coupled system for a period of thousand years after a spin up of 6000 years. The simulation of the mean water mass distribution and the mean circulation of the ocean resembles the observed ocean circulation. It has a warm and fresh bias and the circulation and associated transports are too diffuse and too weak. The ocean's variability is realistic, considering the simplicity of the ocean model, although a bit too weak. We have explored the covariability between the atmosphere and ocean over the Northern Atlantic ocean by performing a singular value decomposition of SST anomalies and 800 hPa geopotential height anomalies. The 2nd mode shows a peak in both spectra at a timescale of about 18 years. The time scale of this mode is set by the ocean but the physical mechanisms that are operating are not yet unambiguously identified. The simulation of this coupled extra tropical decadal mode of variability, which also shows up in the observations and in much more complex coupled models provides strong evidence for the potential usefullness of ECBILT when studying atmosphere/ocean interaction and the associated ocean variability on time scales ranging from decades to many thousands of years.

1. Introduction

The water mass distribution in the oceans and the associated circulation are forced by fluxes of heat, salt and momentum at the surface. These fluxes depend both on the state of the ocean and on the atmosphere and reflect the fact that the systems are coupled. Atmospheric models are frequently run with prescribed ocean surface temperatures. This can be justified as the atmospheric time-scale is so much shorter than the one for the ocean. For ocean models, it is much more difficult

* Corresponding author.

to make a realistic asumption about the atmosphere as the atmosphere adjusts very rapidly to changes in the ocean circulation. Nevertheless many experiments have been performed using either restoring or mixed boundary conditions. In this approach the effect of the stochastic forcing of the ocean by the high frequency transient eddies is neglected. Moreover the dynamic properties of the ocean such as the stability of stationary states, the existence of multiple steady states and the variability may depend crucially on the type of boundary conditions applied. The strong ocean-atmosphere coupling induces atmospheric variations as a response to fluctuations in ocean surface temperatures. These variations will affect the interface fluxes, leading to positive and or negative feedbacks.

The interconnection between climate fluctuations in ocean and atmosphere has been shown with observational data. Time series of Atlantic SST anomalies and atmospheric variables appear to be correlated on decadal time scales (Kushnir, 1994; Folland et al., 1986; Deser and Blackmon, 1993). Grötzner et al. (1996) performed a Canonical Correlation Analysis (CCA) for observed SST and sea level pressure (SLP) data over the North Atlantic. The leading CCA mode showed clear variations on a decadal time scale. The corresponding SLP pattern closely resembles the NAO pattern. The SST pattern is similar to one of the dominant EOFs of SST variability.

Recent simulations with coupled GCM's (Delworth et al., 1993; Von Storch, 1994; Latif and Barnett, 1994; Grötzner et al., 1996; Robertson, 1996) clearly show the existence of a relation between decadal variability in atmosphere and ocean. The associated ocean variability can not entirely be explained by the integration of white noise atmospheric forcing by the ocean leading to red noise SST variability (Hasselmann 1976). Other effects are important and point to an active role for the ocean in the air/sea interaction (Bryan and Stouffer, 1991).

One of the obstacles in modeling atmosphere ocean interaction on decadal timescales is that experiments with GCM's are still fairly expensive. It is possible to run coupled general circulation models for periods of order thousand years, but only one simulation can be performed, which takes usually many months of computer time. This prevents a detailed exploration of the mechanisms behind the slow fluctuations in the ocean. An alternative approach is to develop an atmospheric model that is simple and yet describes the relevant atmospheric feedback processes to the ocean. The possibility of performing many climate simulations under idealized and fully controlled conditions may turn out to be crucial for the unambiguous detection of the feedback processes underlying the simulated variability in the model. In addition the connection of a simple dynamic atmospheric model to an ocean GCM provides the possibility of studying atmosphere/ocean dynamics on very long time-scales of order thousand years. We have developed such a dynamic atmosphere model (ECBILT). We have tested its performance by coupling it to a simple ocean GCM.

ECBILT is a spectral T21 global 3-level quasi-geostrophic (QG) model. The dynamical component of the model was developed by Molteni (Marshall and Molteni, 1993). Forcing a global QG model with an estimate of the observed potential vorticity forcing, which is determined from a long time series of observed streamfunction fields (Roads, 1987), it turns out that both the time mean circulation and its variability can be simulated quite accurately (Marshall and Molteni, 1993; Liu and Opsteegh, 1995; Corti et al., 1997). We have elaborated on this approach by replacing the prescribed potential vorticity forcing with a potential vorticity forcing which is derived from simple parameterization relations. The Molteni model was expanded by including parameterizations for the diabatic processes and for the neglected ageostrophic terms in the vorticity and thermodynamic equations (Haarsma et al., 1997). The latter terms are computed diagnostically from the thermodynamic equation and included as a prescribed time and spatially varying potential vorticity forcing. A similar idea has been put forward by Bengtsson (1974).

The model is 2 orders of magnitude faster than state of the art AGCMs, so it is a very efficient tool for the description of most of the crucial atmospheric feedbacks to the ocean circulation. A serious limitation of ECBILT is that it cannot simulate the observed equatorial variability and consequently the interaction between the tropics and the extra-tropics. So the potential impact of interannual tropical variability associated with ENSO on global climate is neglected.

For the purpose of testing its performance it has been coupled to a simple coarse resolution GFDL type ocean model and a thermodynamic sea-ice model. The coupled model runs on present generation workstations, taking 0.2 h cpu time for the simulation of 1 year (Power Indigo of Silicon Graphics). This report describes the major features of the atmosphere model and summarizes the ocean and the sea-ice model in Section 2. In Section 3 the climate of the atmosphere is described when being run using prescribed climatological sea surface temperatures. In Section 4 the results of two SST anomaly experiments are discussed. Section 5 focusses on the climatology and variability of the ocean when coupled to ECBILT. A decadal coupled mode of North-Atlantic variability is described in Section 6. The results are summarized in Section 7.

2. Description of the model

The climate model contains three separate subsystems (atmosphere, ocean and sea-ice), which exchange heat, moisture and momentum. The dynamical component of the atmospheric model was developed by Molteni (Marshall and Molteni, 1993). The physical parameterisations are similar as in Held and Suarez (1978). For a detailed description of the atmosphere–, ocean- and sea-ice model the reader is referred to Lenderink and Haarsma (1994 and 1996) and Haarsma et al. (1997).

2.1. Atmospheric model: the dynamics

2.1.1. Potential vorticity equation. The dynamical behaviour of the atmospheric model is governed by the quasi-geostrophic potential vorticity equation (Holton, 1992). The equation in isobaric coordinates is:

$$\frac{\partial q}{\partial t} + \boldsymbol{V}_\psi \cdot \nabla q + k_\mathrm{d} \nabla^8 (q - f) + k_\mathrm{R} \frac{\partial}{\partial p}\left(\frac{f_\mathrm{o}^2}{\sigma}\frac{\partial \psi}{\partial p}\right) = -\frac{f_\mathrm{o} R}{c_\mathrm{p}} \frac{\partial}{\partial p}\left(\frac{Q}{\sigma p}\right) - F_\zeta - \frac{\partial}{\partial p}\left(\frac{f_\mathrm{o} F_\mathrm{T}}{\sigma}\right) \quad (1)$$

where q is defined as:

$$q = \zeta + f + f_\mathrm{o}^2 \frac{\partial}{\partial p}\left(\sigma^{-1}\frac{\partial \psi}{\partial p}\right). \quad (2)$$

The variable $\zeta = \nabla^2 \psi$ is the vertical component of the vorticity vector, ψ is the streamfunction, $\boldsymbol{V}_\psi$ is the rotational component of the horizontal velocity, f is the coriolisparameter, f_o is f at 45° north and south, $k_\mathrm{d}\nabla^8(q-f)$ is a highly scale selective diffusion, k_R is a Rayleigh damping coefficient, R is the gasconstant, p is pressure, c_p is the specific heat for constant pressure, $\sigma = -(\alpha/\theta)\partial\theta/\partial p$ is the static stability, α is specific volume, θ is the potential temperature, Q is the diabatic heating, F_ζ contains the ageostrophic terms in the vorticity equation and F_T is the advection of temperature by the ageostrophic wind.

The ageostrophic forcing F_ζ reads:

$$F_\zeta = \boldsymbol{V}_\chi \cdot \nabla(\zeta + f) + \zeta D + \omega \frac{\partial \zeta}{\partial p} + \boldsymbol{k} \cdot \nabla \omega \times \frac{\partial \boldsymbol{V}_\psi}{\partial \boldsymbol{p}} \quad (3)$$

where $\boldsymbol{V}_\chi$ is the divergent component of the horizontal wind, D is the divergence of the horizontal wind, $\omega = \mathrm{d}p/\mathrm{d}t$ is the vertical velocity in isobaric coordinates, and F_T reads:

$$F_\mathrm{T} = \boldsymbol{V}_\chi \cdot \nabla\left(\frac{\partial \psi}{\partial p}\right). \quad (4)$$

Estimates of F_ζ and F_T will be used to represent the effect of the ageostrophic circulation on the tendency of the geostrophic vorticity. This will be explained in the next subsection.

2.1.2. Ageostrophic forcing. We have included the ageostrophic terms F_ζ and F_T in the potential vorticity equation (1) in order to improve the simulation of the Hadley circulation. This appears to have large consequences for the strength and position of the jetstream and for the extra-tropical transient eddy activity. We include these terms by computing the vertical velocity diagnostically from the thermodynamic equation after the temperature tendencies have been computed. Next the horizontal divergence is derived from the continuity equation, using the boundary conditions for ω at the top and bottom of the model atmosphere and the divergent wind $\boldsymbol{V}_\chi$ is derived from the divergence fields. From $\boldsymbol{V}_\chi$ and ω the ageostrophic terms F_ζ and F_T are computed. In the computation of the tendency $\partial\psi/\partial t$ from the potential vorticity equation (1) we use as a first guess the values of F_T and F_ζ as determined in the previous timestep. The tendency $\partial\psi/\partial t$ is computed and the corresponding divergent circulation diagnosed. Computing F_T and F_ζ from this divergent circulation a new estimate for the part of $\partial\psi/\partial t$ forced by the ageostrophic terms is computed. This starts an iteration process. We may iterate until $\partial\psi/\partial t$ has converged. In practice the adjustments in $\partial\psi/\partial t$ after the first iteration are substantially smaller than 10%. After 2 iterations the adjustments are smaller than 1%. For reasons of efficiency we run the model without iterating. So we use the ageostrophic terms from the previous timestep as an additional forcing in ECBILT.

2.1.3. Model discretisation. The model is spectral with horizontal truncation T21. It has three vertical levels, at 800 hPa, 500 hPa and 200 hPa respectively, on which the potential vorticity equation (1) is applied. At the top of the atmosphere ($p=0$ hPa) the rigid lid condition $\omega=0$ is applied. The lower boundary condition for ω is:

$$\omega_s = -\rho_s g\left(\frac{C_d}{f_o}\zeta_s - \boldsymbol{V}_{\psi s}\cdot\nabla h\right), \tag{5}$$

where $\omega_s=(\mathrm{d}p/\mathrm{d}t)_s$ is the vertical motion field and ζ_s and $\boldsymbol{V}_{\psi s}$ are the vorticity and the rotational velocity at the top of the boundary layer respectively, for which we take the values at 800 hPa, C_d is the surface drag coefficient, ρ_s is the density at the surface and h is the orographic height.

2.1.4. Damping timescales. Following Marshall and Molteni (1993) the Ekman dissipation is written as

$$k_E = \frac{\rho_s g C_d}{f_o} = \tau_E^{-1}(1+\alpha_1 LS(\lambda,\phi)+\alpha_2 FH(h)), \tag{6}$$

where τ_E is the Ekman damping time scale, which is assumed to be 6 days. The expression between brackets parameterizes the effect of surface roughness and the orographic height. The fraction of land within a grid box is given by LS and

$$FH = 1-\exp(-h/1000).$$

The α_i are constants: $\alpha_1=\alpha_2=0.5$.

For the scale selective diffusion coefficient we take:

$$k_d = \tau_d^{-1}a^8(21*22)^{-4}, \tag{7}$$

where a is the earth radius. We have chosen τ_d equal to 2 days.

The Rayleigh damping represents the effect of temperature relaxation. For the damping coefficient we have taken $k_R=\tau_R^{-1}$, with $\tau_R=30$ days.

2.2. Atmospheric model: the physics

The diabatic heating is computed from the radiational heating, the release of latent heat and the exchange of sensible heat with the earth. In the following paragraphs we will briefly discuss the parameterisations of these processes.

2.2.1. Vertical profiles. The atmospheric boundary layer is not explicitly resolved by the model. Therefore, in order to compute the heat, moisture and momentum fluxes between the atmosphere and the earth, assumptions about the temperature, moisture and wind profiles in the boundary layer have to be made. For the temperature we assume a linear profile in the logarithm of pressure from the surface to 200 hPa, isothermal above 200 hPa and passing through the computed temperatures at 650 and 350 hPa. We compute the land surface temperature T_s from the assumption of zero heat capacity of the surface, which implies a zero net heat flux F_a between the atmosphere and the land surface. For the moisture we assume that the relative humidity is constant from the surface to the 500 hPa level. The surface wind $\boldsymbol{V}_s$ is assumed to be 0.8 times the wind at 800 hPa, which includes the rotational and divergent component of the wind at that level.

2.2.2. Radiation. The radiation is divided in two bands: a shortwave radiation band for the solar radiation and a longwave radiation band for the terrestrial radiation. Reflection of solar radiation occurs at the top of the atmosphere and the surface. The influence of clouds on the reflection is prescribed and assumed to be a function of latitude only. Absorption is parameterized as a prescribed fraction of the incoming solar radiation. The reflected sunlight from the surface is completely reemitted into space. The surface albedo r_s is determined by the surface characteristics. The different types of surface are land, snow, ocean and sea-ice respectively. The albedos for each surface type are a function of latitude and time of the year.

The long-wave radiation (LW) at the interfaces of the layers is computed according to the parameterization of Held and Suarez (1978). Assuming a constant profile for moisture and the trace gases, they parameterized the LW as computed by the radiation scheme of a GCM. The LW was parameterized as a function of the vertical structure of the potential temperature. The downward flux of

LW at the surface LW_s is computed with the parameterization of Holtslag and van Ulden (1983). The LW emitted by the earth surface is σT_s^4.

2.2.3. Surface fluxes of sensible and latent heat. The evaporation over sea is given by

$$E_{sat} = \rho_a C_d |V_s| (q_s(p_0, T_s) - q(p_0, T_*)),$$

where ρ_a is the air density, C_d is the drag coefficient, $|V_s|$ is the absolute value of the wind speed at anemometer level, q is specific humidity, q_s is saturation specific humidity and T_* is the surface air temperature. Over land the evaporation is reduced proportional to the soil moisture content.

The surface flux of sensible heat SH is given by

$$\mathrm{SH} = \rho_a c_p C_d |V_s| (T_s - T_*).$$

2.2.4. Moisture Budget. The release of latent heat is strongly connected with the transport of moisture and convection. Changes in the specific humidity are described by a single equation for the total precipitable water content between the surface and 500 hPa. Above 500 hPa the atmosphere is assumed to be completely dry. The equation reads:

$$\frac{\partial q_a}{\partial t} = -\nabla_3 \cdot (\boldsymbol{V}_a q_a) + E - P, \tag{8}$$

where q_a is the total precipitable water content between the surface and 500 hPa, $\boldsymbol{V}_a$ the transport velocity for q_a, E evaporation and P precipitation. For the horizontal component of $\boldsymbol{V}_a$ 60% of the sum of the geostrophic and ageostrophic velocity at 800 hPa is taken. The vertical component of $\boldsymbol{V}_a$ is ω_{500}. Moisture which is advected through the 500 hPa plane by the vertical velocity ω_{500} is removed by precipitation which falls through the underlying layer.

Below 500 hPa precipitation occurs when $q_a > 0.8 q_{max}$ where q_{max} is the vertically integrated saturation specific humidity below 500 hPa. The relative humidity r is assumed to be constant throughout the lower atmospheric layer.

Precipitation and convective adjustment were parameterised according to Held and Suarez (1978). The hydrological cycle is closed by using a bucket model for soil moisture. Each land gridpoint is connected to an ocean gridpoint to define the river runoff (Fig.1). Accumulation of snow occurs in case of precipitation when the surface temperature is below zero.

2.3. *Ocean model*

The ocean model is global. The equations are given by the heat and salt budgets, continuity equation, a quadratic equation of state, the hydrostatic approximation, and the horizontal momentum equations. For a detailed description of the ocean model we refer to Lenderink and Haarsma (1994,1996) and Haarsma et al. (1997).

2.3.1. Discretization. The model is discretized on an Arakawa B-grid. It has a uniform depth of 4000 m divided in 12 vertical layers. The vertical velocity w is computed at the intersection between two layers. The atmospheric forcing is added to the two top layers of 30 and 50 m, respectively.

The coarse resolution of the ocean model inhibits a faithfull simulation of the ocean currents in small and shallow seas. Therefore for the Arctic ocean and a few shelf seas like the Mediterranean sea and the sea of Ochotsk, the momentum equations are omitted and in the tracer equations only the diffusive terms and atmospheric forcing are retained. The depth of these diffusive "lakes" is set at 1000 m. They exchange heat and salt with the ocean through diffusivity. The diffusion coefficients for the "lakes" and for the exchange with the ocean can be chosen independently of the diffusion coefficient of the ocean model. At present they are assumed to be equal to the ocean diffusivity. The lakes are depicted in Fig. 1 as areas of light shading. Note that the run off from large continental areas is deposited in the lakes. The fresh water slowly gets into the ocean basin by diffusion.

2.3.2. Boundaries. The no-slip condition and the no-normal flow condition are employed, i.e. the velocities u and v are set to zero on the land-sea boundary. There is no flux of heat and salt across the boundary. For the horizontal advection this is achieved by the no normal flow condition. For horizontal diffusion the normal derivative of the tracer is set to zero.

Due to the absence of bottom topography the Antarctic circumpolar current is strongly underestimated. In order to correct for this deficiency the boundary value of the streamfunction ψ at Antarctica is set to generate a barotropic mass transport of 100 Sv through the Drake passage in the absence of wind forcing.

2.4. *Sea-ice model*

Sea-ice is formed if the ocean temperature drops below -2°C. Sea-ice affects the heat budget of

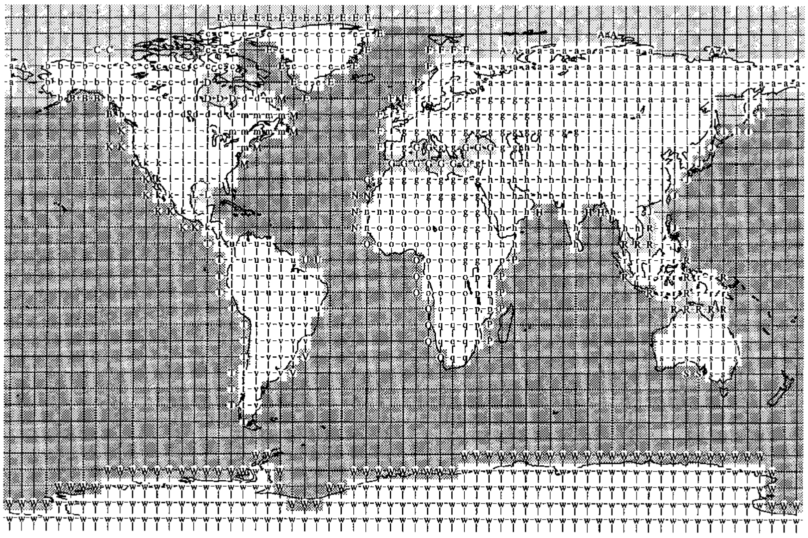

Fig. 1. Land-sea mask of ECBILT. Dark shading corresponds to ocean gridboxes, light shading to lake gridboxes. River runoff in land areas indicated by the same lowercase character is dumped into the sea in the area indicated by the corresponding uppercase character.

the ocean and the atmosphere by strongly reducing the heat exchange between those two subsystems. The salinity budget of the ocean is affected by sea-ice by means of brine rejection and melt water. The effect of sea-ice on the momentum transfer between atmosphere and ocean is neglected. The sea-ice model is based on the zero layer model of Semtner (1976). This model computes the thickness of sea-ice from the thermodynamic balances at the top and the bottom of the ice. The ice model consists of a single layer of sea ice with a variable thickness. On top of the ice there is a variable layer of snow.

2.5. *The coupled model*

The time step of the atmospheric model is 4 h, whereas the ocean model has a time step of 1 day, implying 6 atmosphere time steps for one ocean time step. During these 6 time steps the ocean surface is kept constant. The fluxes of heat, moisture and momentum across the ocean surface are integrated during this period and used during the next time step of the ocean model. The time step of the sea-ice model is chosen to be equal to that of the atmosphere model.

The horizontal discretization of grid points in zonal direction (5.625 degrees) is the same for the scalar gridpoints (T, q, S) of the atmosphere and ocean model. In meridional direction the discretisation is slightly different because of the difference between a regular lat-lon and a Gaussian grid. In this case the values are interpolated. The winds of the atmosphere are interpolated to the vector points of the Arakawa-B grid of the ocean model. The sea-ice model is defined at the scalar points of the ocean model.

3. Climate of the atmosphere model

We have been running the model atmosphere for a period of 500 years with seasonal cycle included both in the solar forcing and in the SSTs. For the solar forcing we used daily averaged values. The climatological SSTs are taken from the COADS dataset (Woodruff et al., 1987).We have evaluated the model results by comparing with observations. The observed mean circulation is taken from the NCEP-NCAR dataset, which is available on CD (Kalnay et al., 1996), and the observed variability is computed from ECMWF analyses for the years 1982 until 1992.

We have evaluated the zonally averaged zonal winds and vertical velocities, the mean geopotential height pattern and the standard deviation of daily geopotential height values at 500 hPa, the simulated potential vorticity forcing, the impact of the ageostrophic terms, the surface fluxes of heat, fresh water and momentum and the leading EOFs of the 500 hPa January mean circulation in the NH.

3.1. *The mean state*

Fig. 2 displays the simulated zonally averaged zonal wind and vertical velocity for winter and summer and their counterparts from the NCEP-NCAR dataset. The simulated jets agree well with the observations. The most significant difference is that the location of the jet maximum in the winter hemisphere lies approximately 10° too far poleward. The strength of the summer jet maximum in the northern hemisphere is substantially too weak and also the easterlies are slightly too weak. The winter jets are accompanied by a Hadley circulation which is too weak and not confined enough in latitudinal extent. Especially the downward branch in the winter hemisphere extends too far into the extra-tropics. This may be the cause for the latitudinal shift of the jet maxima in the winter hemispheres.

Fig. 3 displays the NH winter mean geopotential height at 500 hPa and the standard deviation of daily geopotential height values, both for the model (left) and for the NCEP-NCAR data (right). The simulation of the stationary planetary waves is much too weak. The representation of the variability in the stormtracks is reasonable, although the eddy activity is too weak over the Atlantic.

The reason for the small amplitudes of the

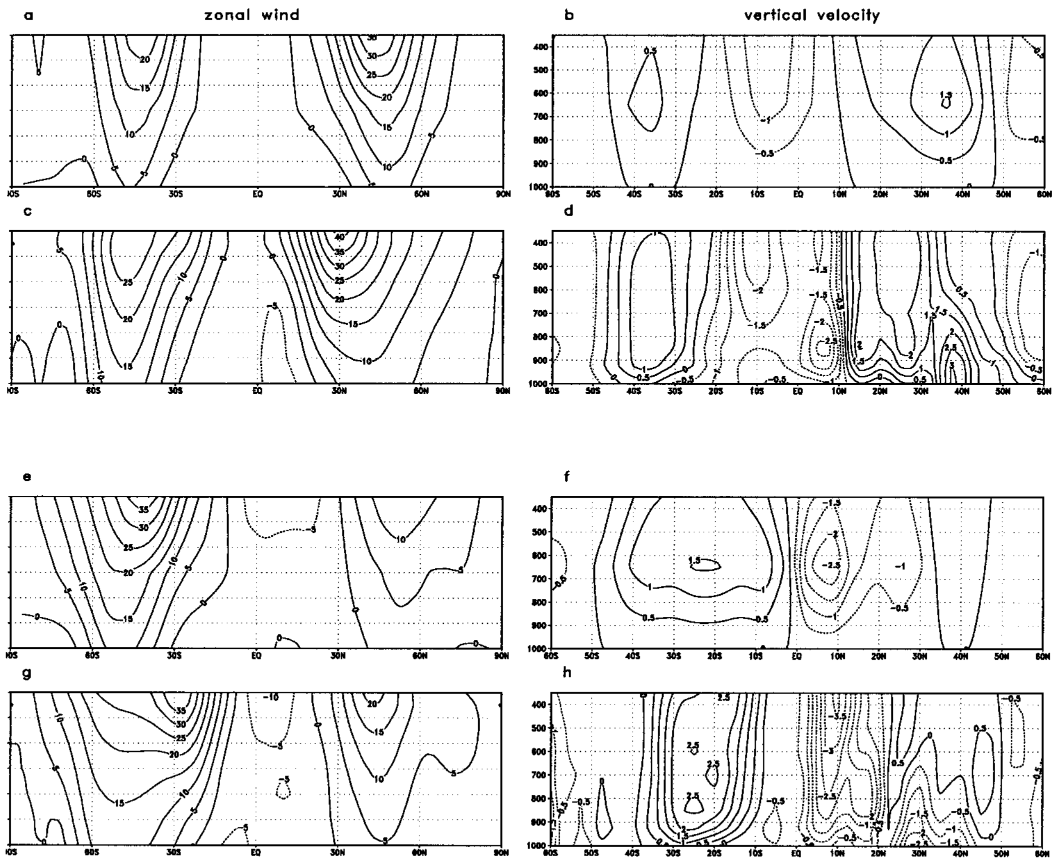

Fig. 2. Simulated zonally averaged zonal wind (m/s) and vertical velocity ω (10^{-3} hPa/s) for winter (a, b) and summer (e, f) and their observed counterparts (c, d and g, h).

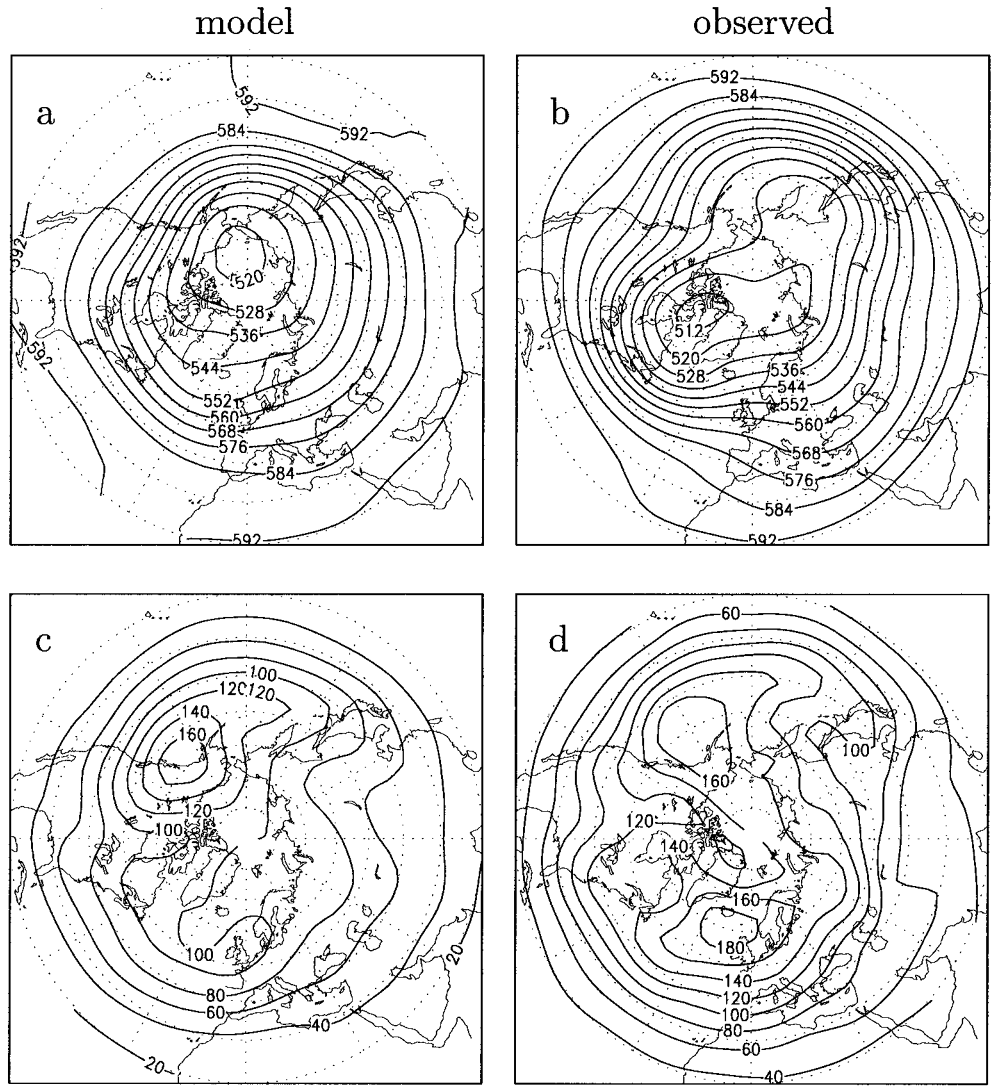

Fig. 3. Winter mean geopotential height at 500 hPa (gpdm) and the standard deviation of daily geopotential height values (m), both for the model (a, c) and for the NCEP-NCAR data (b, d).

planetary scales is not quite clear yet. We have compared the mean potential vorticity forcing as simulated by ECBILT with an "observed" mean potential vorticity forcing. The "observed" forcing was computed from a 10-year dataset of ECMWF data. As suggested by Roads (1987) this forcing can be determined from the observed streamfunction fields by requiring that the tendency in the long-term averaged potential vorticity equation vanishes.The idea has been applied in several papers (Liu and Opsteegh, 1995; Corti et al., 1997). Comparing the simulated January mean potential vorticity forcing with the forcing as computed from the observations, important discrepancies can be noticed. In the "observed" PV forcing strong maxima at latitudes around 30° north and south exist at 200 hPa. These maxima have relatively small scale both in zonal and meridional direction. They dominate the "observed" PV forcing field, but are weak in the PV forcing field of

ECBILT. Forcing the QG model with the "observed" PV forcing field, an almost perfect climatic mean state and standard deviation of daily geopotential height results. The "observed" forcing does not only reflect the diabatic forcing, but also includes the effect of everything that is neglected into the QG equations (the effect of the unresolved geostrophic modes onto the resolved modes and the effect of the neglected ageostrophic terms). So at present the reason for this major discrepancy between "observed" and simulated PV forcing is not clear. We suspect that the interaction of the ageostrophic component of the tropical Hadley circulation with the extra-tropical planetary-scale geostrophic circulation is not well resolved by the indirect procedure of including the ageostrophic terms as described in Subsection 2.1.2. This procedure only works if the ageostrophic terms are small as compared to the geostrophic terms. This requirement is not satisfied in the tropics. In spite of this shortcoming it appears that the overall improvements on the quality of the simulation by including the ageostrophic terms are substantial. We have tested this by repeating the simulation without these terms. The jet strength and the stormtracks appear to be significantly weaker. In particular the latitudinal extent of the winter jet is much too broad without these terms and the jet maximum becomes $10\ \mathrm{ms}^{-1}$ weaker.

The model has been developed as an alternative to the frequently used mixed boundary conditions for ocean models, so that mechanisms for oceanic extra-tropical long term variability can be studied taking to first order into account the physical and dynamical atmospheric feedback processes. This means that we demand that the model generates realistic surface fluxes. Fig. 4 displays the zonal mean E-P fluxes for the NH winter and summer both for the model and the NCEP-NCAR data. The agreement with the observations is striking, especially for the summer hemispheres. In the winter hemispheres the positive E-P fluxes at approximately 20°N and 20°S are substantially weaker than observed. The negative E-P fluxes north of 70°N in the NH summer are too large. Fig. 5 displays the distribution of the NH winter mean precipitation, the total surface heat flux and the zonal wind at 800 hPa for the model and the NCEP-NCAR data. The simulation of the precipitation distribution is quantitatively in very good agreement with the observations. The amount of rainfall in the NH stormtracks is a little too weak and the tropical ITCZ is partly missing, but the location of the areas of maximum precipitation is comparable to the results of much more complex models.

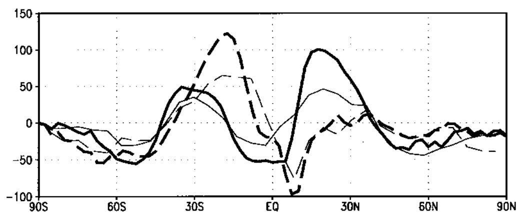

Fig. 4. Zonal mean E-P fluxes (cm/year) for winter (solid lines) and summer (dashed lines) both for the model (thin lines) and the NCEP-NCAR data (thick lines).

The simulated sensible and latent heat fluxes (not shown) compare similarly well with the NCEP-NCAR data. Here we show the total surface heat flux, which is the sum of absorbed solar radiation, emitted infrared radiation and the sensible and latent heat fluxes. The simulated heat flux is in good agreement with the NCEP-NCAR data, although local discrepancies exist.

The surface stresses must be parameterized from the 800 hPa winds. At present the parameterization relation is very crude and can substantially be improved. In the coupled simulation we have taken the surface winds to be 0.8 times the 800 hPa winds, without rotating the wind vector (in order to include the effect of the Ekman friction) and without distinguishing between land and ocean or taking into account the surface elevation. For this reason we display here the simulated 800 hPa zonal wind distribution. The figure shows that the areas of maximum westerly zonal winds are over the extra-tropical oceans at approximately the right latitudes (with the exception of the northern Pacific maximum, which is located too far to the north) and with amplitudes which are slightly too weak. The area of tropical easterlies extends too far into the extra-tropics.

3.2. *Variability*

Fig. 6 displays the four leading EOFs for the January mean 500 hPa circulation in the Northern Hemisphere. The calculations were based on 500 January mean circulation patterns. The EOFs

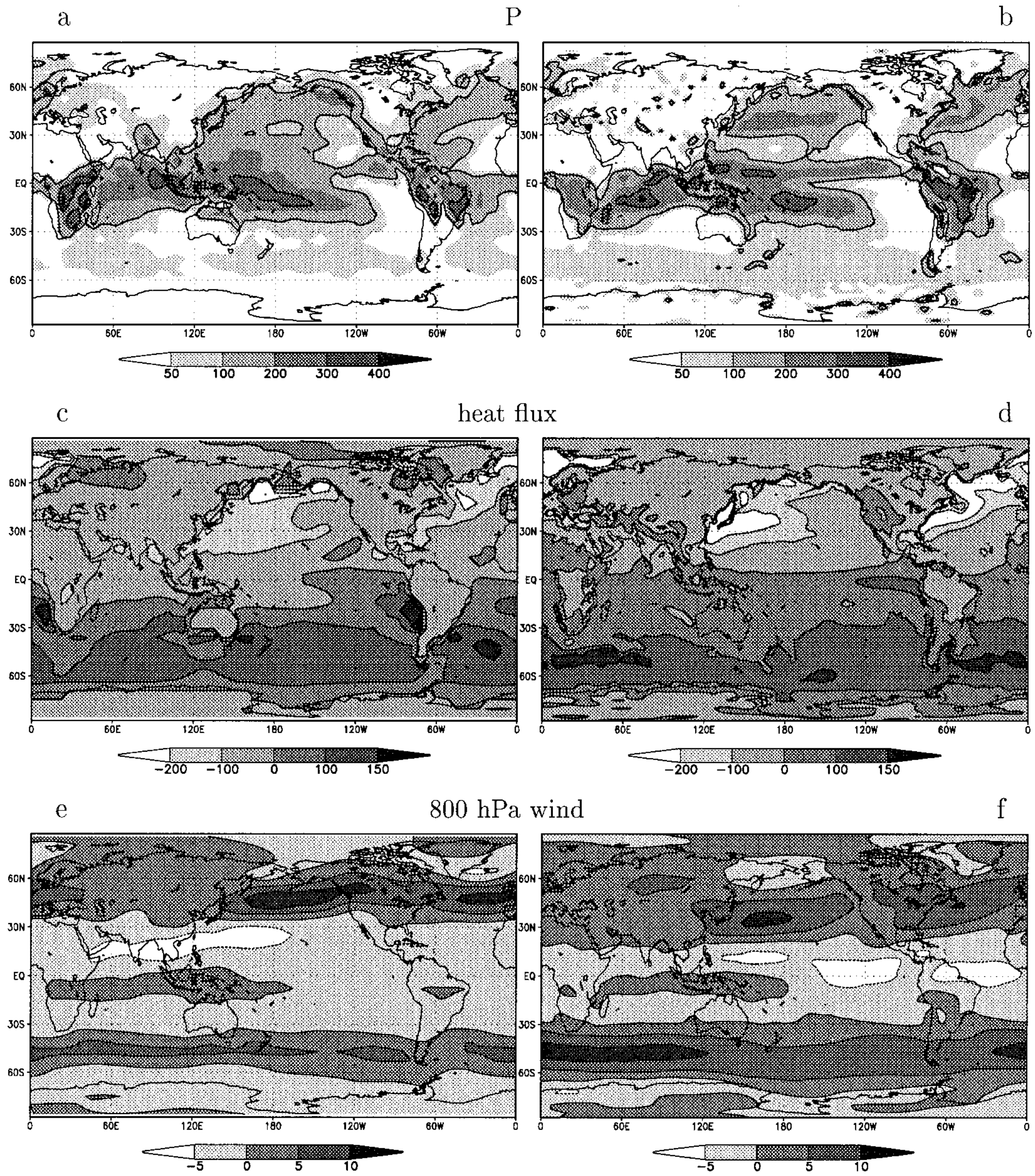

Fig. 5. Distribution of winter mean precipitation (cm/year) (a), net surface heat flux (W/m^2) (c) and 800 hPa wind (m/s) (e) and the corresponding fields from the NCEP-NCAR data (b,d,f).

explain 26%, 11%, 10% and 7% of the variance in the monthly mean patterns respectively. The first two EOFs have wavelike structures reminiscent of the observed PNA teleconnection pattern. In the EOFs 3 and 4 the variability over the Northern Atlantic and European area dominates. EOF 4 resembles the observed NAO pattern. We have compared the simulated patterns with observed EOFs computed from the 10 years of ECMWF data. The EOFs have strong similarities with the observed patterns computed from 10 January means only, although a substantial

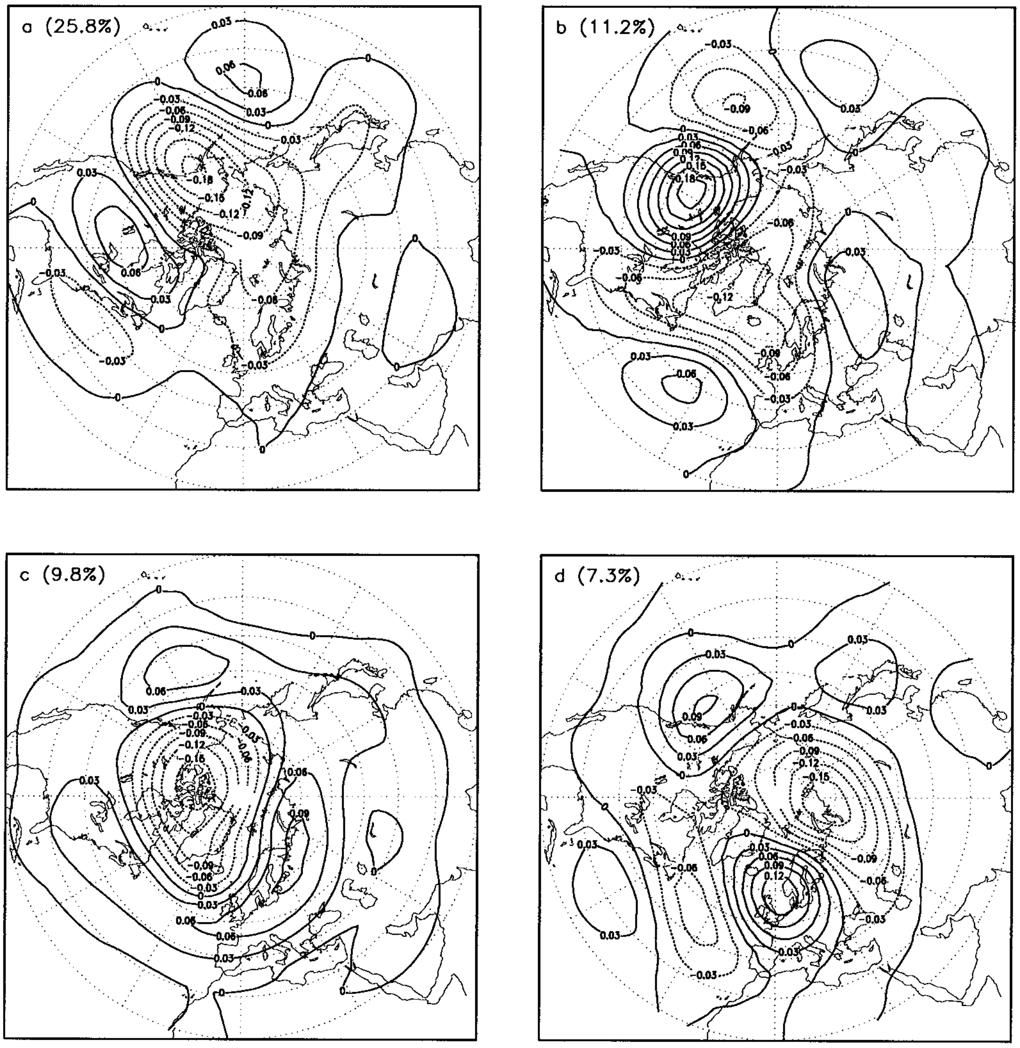

Fig. 6. The four leading EOFs for the January mean 500 hPa circulation in the NH.

amount of mixing exists. The simulated variability over the Northern Atlantic and European area is too small. The explained variance in EOF 3 and 4 is only 10% and 7% respectively. The observed EOFs 1 and 2 as computed from the ECMWF data have a substantial amplitude in the Northern Atlantic. They explain 30% and 24% of the variance of the ECMWF dataset, although in these figures a substantial statistical sampling effect may be present. Nevertheless it is clear (especially from the simulated standard deviation as shown in Fig. 3) that the model underestimates the strength of the variability over the North Atlantic, which may be caused by the weak amplitudes of the planetary scale waves, especially the almost absence of the Icelandic low.

4. Response to SST anomalies

In order for the atmosphere model to provide the proper boundary conditions to the ocean, it should produce an acceptable response to SST anomalies, otherwise it can not be expected that the important feedbacks to the ocean are well resolved. We expect that the response to tropical SST anomalies will be poor but that the response to extra tropical anomalies is realistic. We have tested this hypothesis by performing two SST anomaly experiments, one with a tropical SST anomaly and one with an SST anomaly in the northern extra-tropical Atlantic ocean. In order to simulate the response to the SST anomalies we have performed a control run and a perturbation run.

For the tropical SST anomaly experiment we used the tropical Pacific SST anomaly as observed during January 1983. The experiment was performed for perpetual January conditions. Both the control and the perturbation run were integrated for 3600 days, starting from an arbitrary January initial state. We did not use the first 360 days in the analysis of the results. Fig. 7 displays the response at the 500 hPa level. Although the amount of anomalous precipitation agrees well with what has been found with atmospheric GCM's, the resulting extra-tropical teleconnection pattern is very weak (Blackmon et al., 1983).

Held and Kang (1987) analysed the mechanisms causing the extratropical response to tropical heating in a low resolution GCM by forcing a barotropic model with divergence patterns which were derived from the GCM simulation. They found that not the tropical but the subtropical anomalous divergence patterns were crucial in order to reproduce the GCM's anomalous response. These subtropical divergence patterns must be an indirect result of the tropical anomalies and may have been generated by anomalies in the local ageostrophic overturning circulations. As was already noticed when discussing the simulation of the climatological stationary waves the QG model is deficient in reproducing these strong subtropical divergence patterns. In Kok and Opsteegh (1985) and Held et al. (1989) the importance of extratropical anomalous transient feedback on to the planetary scale circulation was shown. However when the effect of the divergence forcing from the subtropics is severely underestimated, it is not surprising that extratropical transient feedbacks will also be small. So we must conclude that this model cannot deal adequately with extratropical climate variability resulting from interaction with the tropics.

The response to SST anomalies in the middle latitudes was investigated with an SST pattern that was derived from a singular value decomposition (SVD) analysis of 800 hPa geopotential height and SST that was applied to the results of the 1000 year coupled integration. From the 1000 year integration we selected a winter with a large positive phase of the second SVD pair and a winter with a large negative phase. The difference between the two winter mean SST patterns is plotted in Fig. 8a. It is very similar to one of the dominant patterns of observed decadal Atlantic

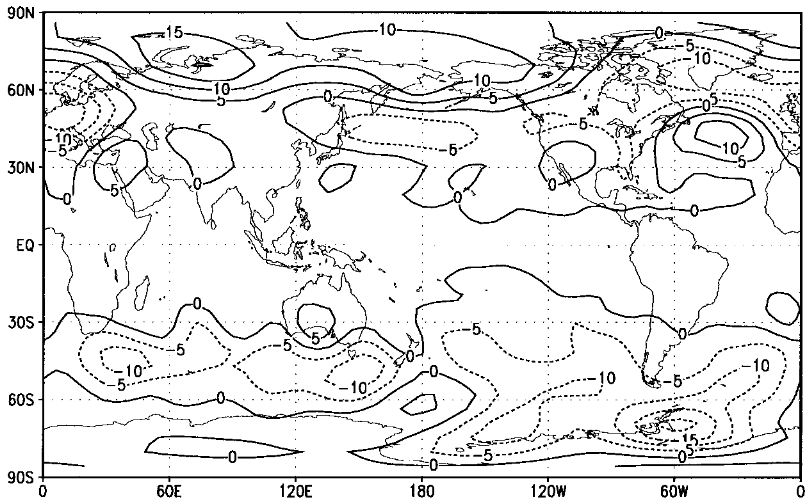

Fig. 7. Anomalous 500 hPa teleconnection pattern (m) for the tropical SST anomaly experiment.

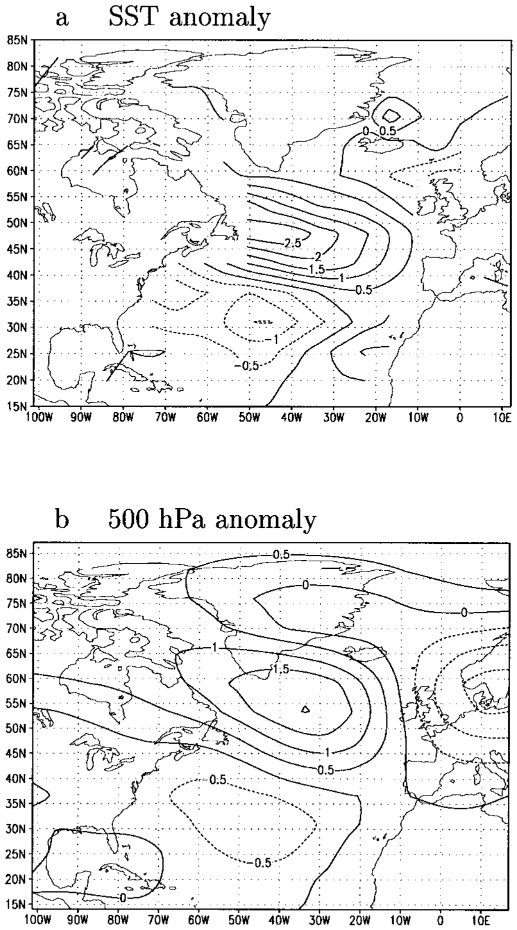

Fig. 8. Winter mean SST difference between the two atmosphere only runs in the extra tropical SST experiment (a) and 500 hPa geopotential height response (gpdm) (b).

SST variability as described by Deser and Blackmon (1993). The maximum SST difference is about 2 K. Of these two winters (from July preceding the winter until June next year), the daily global model SSTs were used as a lower boundary condition. We performed two 40-year atmosphere only integrations. A climatological sea-ice cover, calculated from the first 100 years of the coupled run, was used in both atmosphere only integrations. The last 30 years were used to calculate the difference in climatology between both runs. The DJF atmospheric surface air temperature (not shown), displays a response in the order of 1 K, with an almost identical structure as the SST anomaly pattern. The positive surface air temperature anomaly has shifted slightly downstream of the maximum positive SST anomaly. A negative response is found on top of the negative SST anomaly at 30°N, 50°W. A negative response is also seen over North-Western Europe. The difference in the DJF geopotential height fields at 500 hPa is in the order of 15 m (Fig. 8b). Differences in surface wind values are somewhat smaller than 1.0 m/s. The atmospheric response pattern agrees well with similar SST anomaly experiments performed with atmospheric GCM's by Palmer and Sun (1985) and Ferranti et al. (1994). In these studies the amplitude of the response seems to be somewhat larger, which may be partly caused by the fact that the simulations in these two papers were done for a few seasons only, which probably does not entirely separates the response pattern from the internally generated noise. Also the weakness of the climatological stationary waves in the present model simulation (Fig. 3), especially in the Atlantic region must play a role. It has been shown in a number of papers that the amplitude of the midlatitude reponse to a forcing of given amplitude is increasing with increased amplitude of the stationary waves. Future attempts will be undertaken to improve the simulation of the climatological standing wave pattern.

5. Climatology and variability of the ocean.

Starting from a state of rest and an idealized temperature distribution, the coupled system was integrated for 6000 years. In this section we will describe the mean state and variability of the ocean as analysed from the last 1000-years. During the spin up we did some minor tuning to reduce the global warming trend that occurred. As can be seen from Fig. 4 the fresh water flux in the Arctic, especially during NH summer is too big. This causes the thermohaline circulation to partly collapse. We decided to apply a correction to the fresh water flux north of 75°N. In this area the flux to the ocean was reduced to 20% of its computed value. After this change the overturning circulation increased to a mean value of about 13 Sv.

5.1. Climate of the ocean

After 6000 years of spinning up the deep ocean did not yet reach an equilibrium climate: the deeper layers show a slow drift in temperature ($6 \cdot 10^{-3}$ K/year) and salinity ($-1.4 \cdot 10^{-4}$ psu/year). The ocean is too warm and too saline, especially at intermediate depth. The vertical structure of the globally averaged temperature and salinity profiles with depth, show the main thermocline and different main watermasses, but more diffuse than in state-of-the-art OGCMs or reality.

A salinity section at 30W in the North Atlantic basin (Fig. 9) shows the signatures of the watermasses: Relatively warm surface water, fresh in the tropics and subpolar regions and saline in the subtropical gyres. Fresher Antarctic intermediate water coming from the south and an inflow of rather salty NADW from the north. There is here no clear hint of AABW near the bottom which should be flowing northward beyond the equator, but the meridional overturning streamfunction (not shown) demonstrates its presence in the model. There is a large scale, qualitative, correspondence to the real ocean, while the more detailed regional distribution and the properties of the watermasses are rather different from what is observed.

The temperature T and salinity S at ~ 120 m depth (not shown) show the general structure of the net surface heating, modified by the wind driven circulation and the thermohaline circulation (a warmer and saltier North Atlantic relative to the North Pacific, especially in the east), similar to observations. There is little structure in the equatorial oceans, as may be expected from the deficiencies in the simulation of the atmospheric equatorial dynamics. Simulated features in the extra-tropics are qualitatively similar to observations.

Watermass formation at high latitudes in the North Atlantic, driven by atmospheric cooling of the relatively salty waters, is evident in the simulation. About 12 Sv of "model NADW" sinks at high latitudes, somewhat less than observed. Part of this cooled surface water flows back into the South Atlantic ocean below the surface (~ 6 Sv in the model) forming a link in the "global ocean conveyor-belt" of the model. This flow pattern also causes the net northward heatflow through both South and North Atlantic. A negative "overturning cell" near the bottom at the equator indicates the influence of AABW, even though this watermass is not apparent in the salinity/temperature structure. The wind driven

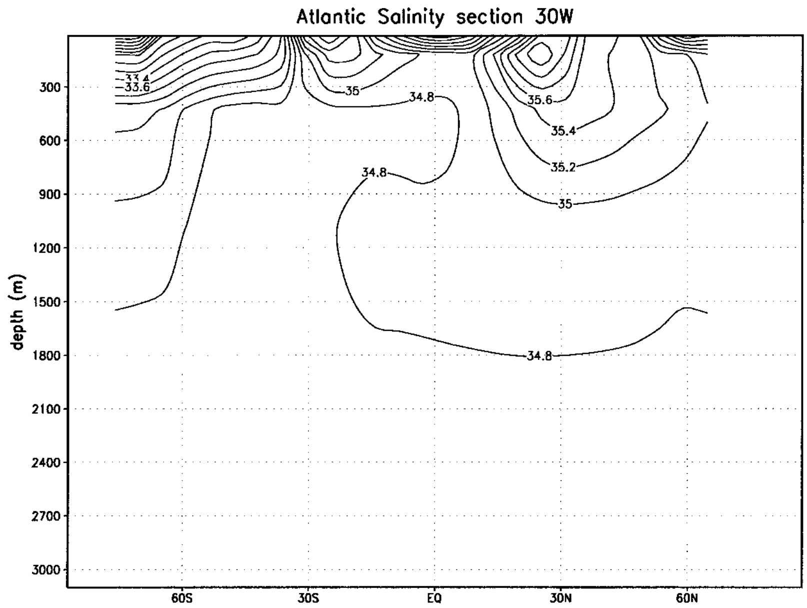

Fig. 9. Vertical salinity distribution in the North Atlantic along 30°W.

subtropic and subpolar gyre circulations are rather weak, especially the western boundary currents.

5.2. *Global SST variability*

Apart from the seasonal cycle in the globally averaged SST for DJF, which is about 0.2°C, year to year and longer term variability with amplitude of about 0.1°C is apparent in the coupled run. Compared to observations, both these numbers are of the right order of magnitude, albeit rather low. It should be kept in mind that there is no variability in the solar forcing apart from the seasonal cycle. The variance spectrum of 1000 year global NH-winter SST is shown in Fig. 10. The red character of the SST variability is well documented in the literature (Frankignoul and Hasselmann, 1977) and is the consequence of the mechanism described by Hasselmann (1976) where the oceans, with large heat capacity and relatively slow dynamics, act as integrator of the rapidly varying atmospheric forcing. The peak at the low frequency end of the spectrum has approximately a 64 years period. It is significantly different from a red noise spectrum at the 95% confidence level. The peak is associated with large scale variability in the Southern Ocean. The confidence limits were estimated from a Monte-Carlo simulation of 100000 spectra of AR(1) timeseries of the same length as the analysed timeseries (1000 points). The parameters of the AR(1) process were determined from the autocorrelation coefficient at lag 1 year and the total variance of the timeseries.

5.3. *North Atlantic variability*

The variance spectrum of the NH-winter North Atlantic meridional overturning is shown in Fig. 11. Again we see variability in a wide range of timescales, from interannual to interdecadal. Simulated variations of several Sverdups are comparable with similar thermohaline variability in a state-of-the-art coupled Ocean-Atmosphere model that was described by Delworth et al. (1993). A very prominent peak in the spectrum appears at a time scale of approximately ten years. The physics behind this peak is not clear yet, but will be one of the subjects of a future paper.

In Fig. 12, the standard deviation of the SSTs in the North-Atlantic basin as calculated from the 1000-year run and the 90-year GISST (Global Ice and Sea Surface Temperature) dataset is shown. The GISST data is provided by the British Meteorological Office and comprises the years 1903–1993. The calculations were based on winter half-year mean fields (ONDJFM). Any linear trend in the observations was removed at each gridpoint.

The model variability is slightly less than observed. Both observations and model show

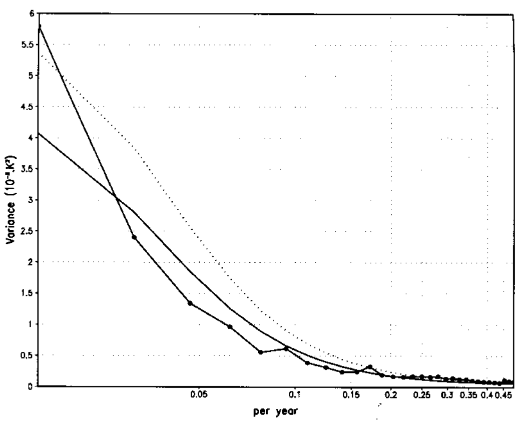

Fig. 10. Power spectrum of globally averaged winter mean SST. The unmarked lines correspond to the spectra of a fitted AR(1) process (solid) and the 95% confidence limit (dotted) determined from 100 000 Monte-Carlo simulations.

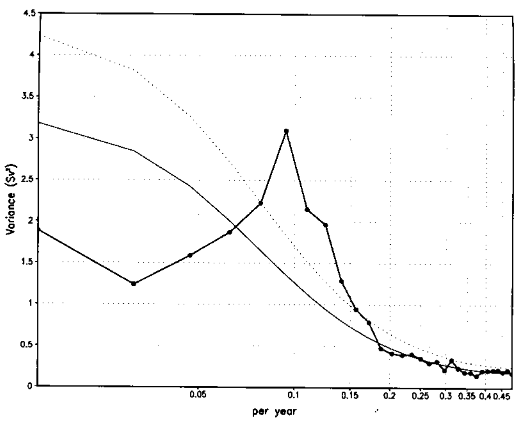

Fig. 11. Power spectrum of maximum meridional overturning in the North Atlantic ocean. The unmarked lines correspond to the spectra of a fitted AR(1) process (solid) and the 95% confidence limit (dotted) determined from 100 000 Monte-Carlo simulations.

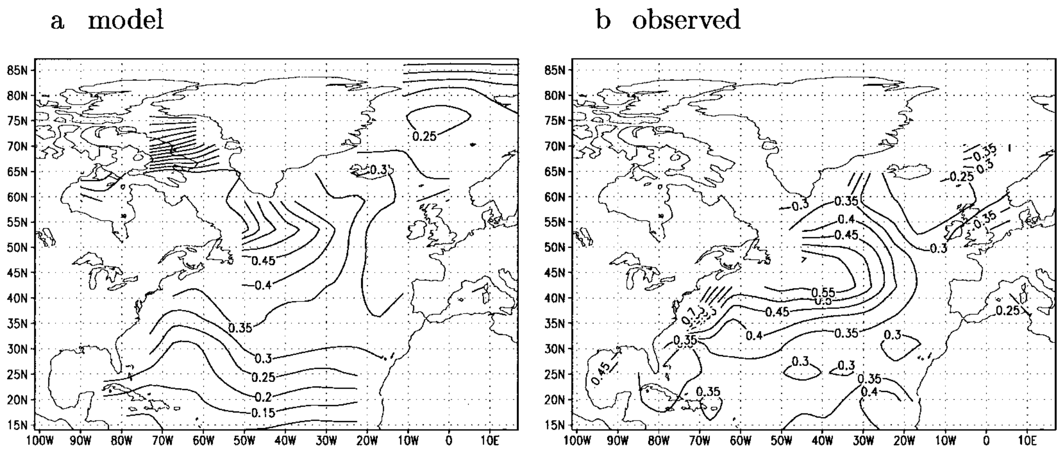

Fig. 12. Simulated (a) and observed (b) standard deviation of SST in the North-Atlantic basin based on winter half-year mean fields (ONDJFM).

maximum variability located off the East coast of North-America, extending eastward between 40° and 60° North. The model maximum has shifted to the north by about 10°. In contrast to the observations the variability in the model decreases monotonically equatorward of 30° North.

EOFs were calculated from the NH-winter mean fields for both the GISST and the model data. The first four EOFs acount for about 60% of the variance in both datasets. In Fig. 13, the first two EOFs are plotted for both the observations and the model. The first GISST EOF represents a basin wide warming or cooling, which is not reproduced in the model. GISST EOFs 2 and 3 are characterized by north-south oriented dipole structures as are model EOFs 1,2 and 3. GISST EOF 4 is characterized by an east-west oriented sequence of positive and negative anomalies and compares well with model EOF 4. Due to the short observational record, the individual observed EOFs can not yet be well resolved. This must be particularly true for GISST EOFs 2 and 3 for which the eigenvalues are about the same.

6. A decadal coupled mode of variability of the North-Atlantic

To explore the connection between variations in the atmosphere and the ocean, a Singular Value Decomposition (SVD) was made for the area shown in Fig. 14 of winter mean SST anomalies and 800 hPa geopotential height anomalies. The second SVD pair is plotted in Fig. 14. A short timeseries of the amplitudes to give an impression of the temporal evolution is plotted in Fig. 15 along with a power spectrum estimate of these timeseries. The SST pattern (Fig. 14a) projects mainly onto SST EOFs 2 and 3, whereas the Φ_{800} anomaly pattern (Fig. 14b) resembles the models equivalent of the NAO pattern. Consistent with the results of for instance Verbeek (1997), warmer (colder) than normal SSTs coincide with weaker (stronger) than normal westerly winds. A clear decadal signal is visible in both the SST variance spectrum (Fig. 15b) and to a lesser extend in the Φ_{800} spectrum (Fig. 15c) at a timescale of about 18 years. The peaks are significantly different from a red noise spectrum at the 95% confidence level. In the timeseries (Fig. 15a) the 18 year period is clearly visible in both the SST variations (solid line) as well as in the Φ_{800} variations. The temporal correlation between both timeseries is 0.7. Note that no filtering was applied to remove the interannual variability that is also clearly present in the timeseries. The variability of the first and third SVD pairs (not shown) do not peak at decadal timescales; the SST variations are indistinguishable from red noise, whereas the variance spectra of the Φ_{800} variations are white. The second SVD mode is similar to the mode found by Grötzner et al. (1996) in the ECHO coupled integration (their Fig. 3) and in their analysis of observed SST and SLP data (their Fig. 4). The SLP patterns

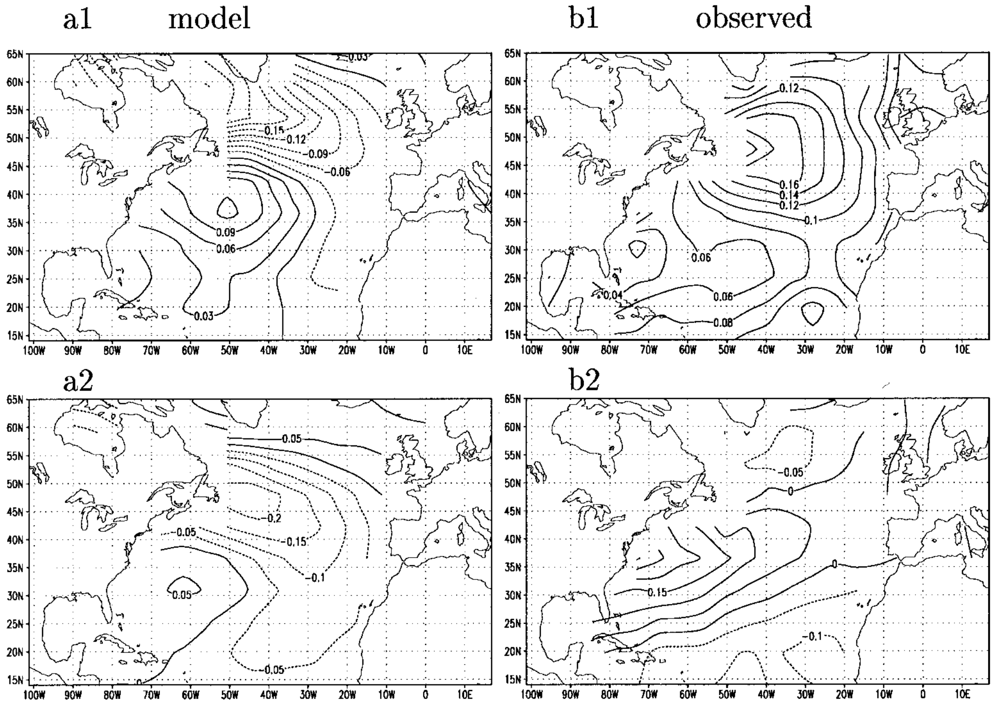

Fig. 13. Simulated (a) and observed (b) EOF patterns of North Atlantic SST.

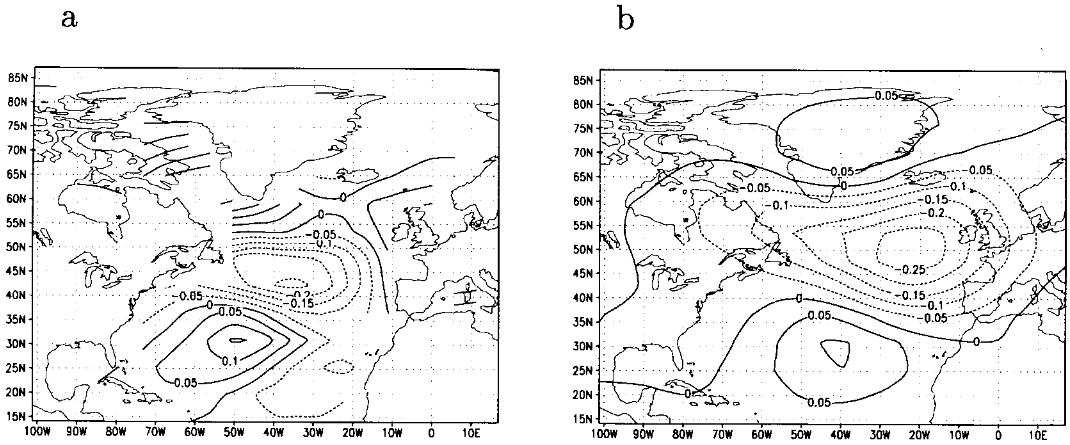

Fig. 14. Second SVD mode of SST and Z_{800} for the 1000-year coupled integration: (a) SST pattern, (b) Z_{800} pattern.

look like NAO and describe variations in strength of the westerlies. The ECHO mode peaks at about 18 years, the observed mode around 12 years. (We used an SVD analysis rather than a Canonical Correlation Analysis (CCA), since the CCA modes turned out to be very sensitive to the number of EOFs used in the analysis, see also Bretherton et al., 1992). Both the patterns, as well as the timescale suggest that ECBILT simulates a similar decadal mode of variability as the ECHO coupled

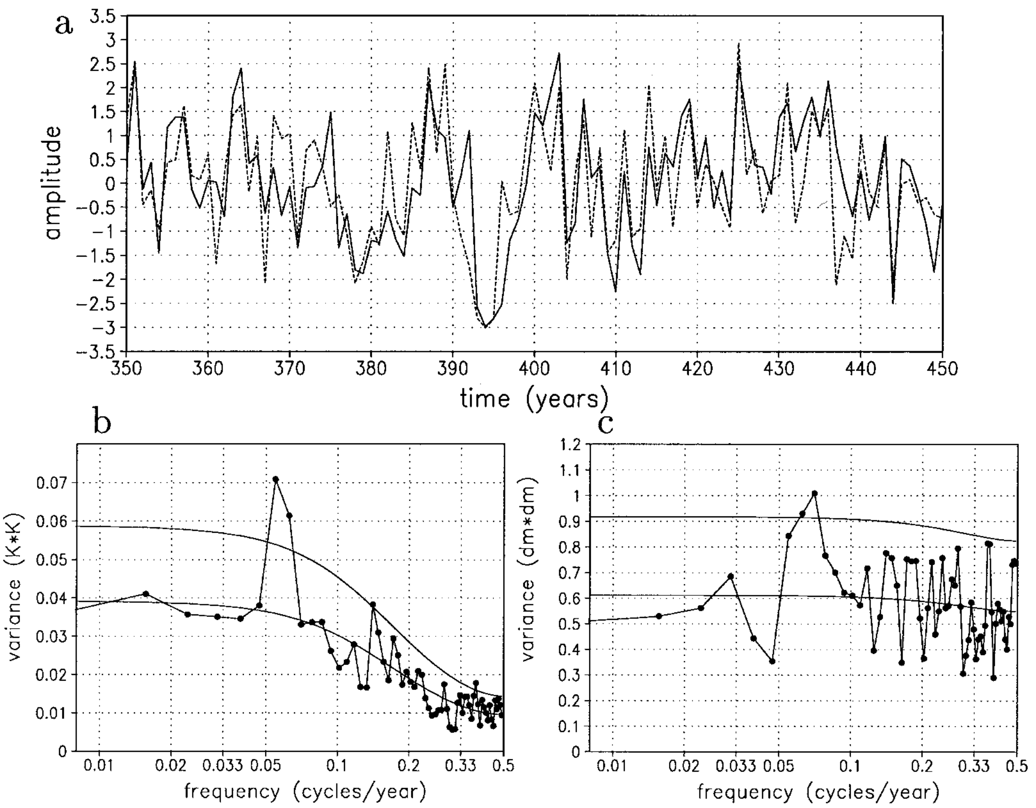

Fig. 15. Second SVD mode of SST and Z_{800} for the 1000-year coupled integration: (a) time series of SST (K) (solid line) and Z_{800} (5 m) (dotted line), (b) variance spectrum SST (K^2) and (c) variance spectrum Z_{800} (dm^2). The unmarked lines in (b) and (c) correspond to the spectra of a fitted AR(1) process and the 95% confidence limit determined from 100 000 Monte-Carlo simulations.

GCM. In a forthcoming paper the physics behind this coupled decadal mode of variability will be analysed. In this analysis, we made extensive use of the possibility to perform many additional simulations under idealised and controlled conditions. These simulations appear crucial in order to be able to firmly establish the relevant physical processes.

7. Summary

As an alternative to the frequently used mixed boundary conditions in ocean GCM's we have developed a dynamic atmospheric model (ECBILT) that is simple and yet describes the relevant dynamic and thermodynamic feedback processes to the ocean. This provides the possibility of studying atmosphere/ocean dynamics on very long time-scales of order thousand years.

ECBILT is a spectral T21 global three level quasi-geostrophic model with simple parameterizations for the diabatic processes (Haarsma et al., 1997). The model is realistic in the sense that it contains the minimum amount of physics that is necessary to simulate the mid-latitude planetary and synoptic-scale circulations in the atmosphere as well as its variability on various time-scales. It can be used to study the fundamental nature of air/sea interaction in the extratropics. As an extension to the quasi-geostrophic equations, an estimate of the neglected ageostrophic terms in the vorticity and thermodynamic equations is included as a time and spatially varying forcing.

The model is two orders of magnitude faster than AGCMs.When coupled to the ocean GCM it runs on present generation workstations, taking 0.2 h cpu time for the simulation of 1 year (Power Indigo of Silicon Graphics).

We have been running ECBILT with prescribed SSTs for a period of 500 years with seasonal cycle included both in the solar forcing and in the climatological SSTs. The mean state and the variability properties of ECBILT are reasonably realistic, although discrepancies with the observed atmospheric state occur. The simulation of the surface fluxes is realistic and justifies coupling ECBILT to an ocean GCM, making a detailed search for the potential impact of extra-tropical atmosphere/ocean interaction processes for the observed ocean variability feasible on time scales ranging from decades to many thousands of years.

In order for the atmosphere model to provide the proper boundary conditions to the ocean, it should produce an acceptable response to SST anomalies, otherwise it can not be expected that the important feedbacks to the ocean are well resolved. We have done two SST anomaly experiments, one with a tropical SST anomaly as observed during January 1983 and one with an SST anomaly in the northern extra-tropical Atlantic ocean. For the tropical SST anomaly experiment the amount of anomalous precipitation agrees well with what has been found with atmospheric GCM's, but the resulting extra-tropical teleconnection pattern is very weak. So we must conclude that this model cannot deal adequately with extratropical climate variability resulting from interaction with the tropics. The atmospheric response pattern to extra-tropical SST anomalies agrees well with similar SST anomaly experiments performed with atmospheric GCM's by Palmer and Sun (1985) and Ferranti et al. (1994). In these studies the amplitude of the response seems to be somewhat larger, which may be caused by the fact that the simulations in these two papers were done for a few seasons only, which probably does not entirely separates the response pattern from the internally generated noise.

We have tested the performance of ECBILT in coupled mode by coupling it to a simple ocean GCM and thermodynamic sea-ice model and integrating the coupled system for a period of thousand years after a spin up of 6000 years. We have analysed the mean state and the variability properties of the ocean in the thousand year run. The simulation of the mean water mass distribution and the mean circulation resembles the observed ocean circulation. It has a warm and fresh bias and the circulation and associated transports are too diffuse and too weak. The ocean's variability is realistic, considering the simplicity of the ocean model, although a bit too weak.

We have explored the covariability between the atmosphere and ocean over the Northern Atlantic ocean by performing a singular value decomposition of SST anomalies and 800 hPa geopotential height anomalies. The second mode shows a peak in both spectra at a timescale of about 18 years. The time scale of this mode is set by the ocean but the physical mechanisms that are operating are not yet unambiguously identified. It shows very good correspondence with the coupled mode found by Grötzner et al. (1996) in the ECHO coupled integration.

The simulation of this coupled extra tropical decadal mode of variability, which also shows up in the observations and in much more complex coupled models provides strong evidence for the potential usefullness of ECBILT when studying atmosphere/ocean interaction and the associated ocean variability on time scales ranging from decades to many thousands of years.

8. Acknowledgements

Selten was supported by the Dutch National Research Programme on Global Air Pollution and Climate Change, registered under nr. 951208, titled: "Climate Variability on Decadal Timescales". We acknowledge the programming support by Qing Liu. He was supported by the EC in the context of the programme "Environment and Climate", project: "Decadal and Interdecadal Climate Variability: Dynamics and Predictability Experiments" (DICE), projectnr. EV5V-CT94–0538. We thank Dr. S. Weber for carefully reading the first draft of this paper and for providing valuable comments.

REFERENCES

Bengtsson, L. 1974. *A three parameter model for limited area forecasting*. Techn. Paper No. 5–74. Naval Postgraduate School, Monterey, California 93940.

Blackmon, M. L., J. E. Geisler and E. J. Pitcher, 1983. A general circulation model study of January climate anomaly patterns associated with interannual variation of equatorial Pacific sea surface temperatures. *J. Atmos. Sci.* **40**, 1410–1425.

Bretherton, C. S., C. Smith and J. M. Wallace, 1992. An intercomparison of methods for finding coupled patterns in climate data. *J. Climate*. **5**, 541–560.

Bryan K. and R. Stouffer, 1991. A note on Bjerknes' hypothesis for North Atlantic variability. *J. Mar. Sys.* **1**, 229–241.

Corti, S., A. Giannini, S. Tibaldi and F. Molteni, 1997. Patterns of low frequency variability in a three level Quasi-Geostrophic model. *Climate Dynamics*, in press.

Delworth, T., S. Manabe, R. J. Stouffer, 1993. Interdecadal variations of the thermohaline circulation in a coupled ocean-atmosphere model. *J. Climate* **12**, 1993–2011.

Deser, C. and M. L. Blackmon, 1993. Surface climate variations over the North Atlantic Ocean during winter 1900–1989. *J. Clim.* **6**, 1743–1753.

Drijfhout, S., C. Henze, M. Latif and E. Maier-Reimer, 1996. Mean circulation and internal variability in an ocean primitive equation model. *J. Phys. Oceanogr.* **26**, 559–580.

Ferranti, L., F. Molteni and T. N. Palmer, 1994. Impact of localized tropical and extratropical SST anomalies in ensembles of seasonal GCM integrations. *Q. J. R. Meteorol. Soc.* **120**, 1613–1645.

Folland, C. K., T. N. Palmer and D. E. Parker, 1986. Sahel rainfall and worldwide sea temperatures, 1901–85. *Nature* **320**, 602–607.

Frankignoul, C. and K. Hasselmann, 1977. Stochastic climate models. Part II. Application to sea-surface temperature anomalies and thermocline variability. *Tellus* **29**, 289–305.

Grötzner, A., M. Latif and T. P. Barnett, 1996. *A decadal climate cycle in the North Atlantic ocean as simulated by the ECHO coupled GCM*. Max-Planck-Institut für Meteorologie. Report No. 208.

Haarsma, R. J., F. M. Selten. J. D. Opsteegh, G. Lenderink and Q. Liu, 1997. *ECBILT: A coupled atmosphere ocean sea-ice model for climate predictability studies*. KNMI technical report TR-195, De Bilt, The Netherlands.

Hasselmann, K. 1976. Stochastic climate models. Part I. Theory. *Tellus* **28**, 473–485.

Held, I. M. and M. J. Suarez, 1978. A two level primitive equation atmosphere model designed for climate sensitivity experiments. *J. Atmos. Sci.* **35**, 206–229.

Held, I. M. and I. S. Kang, 1987. Barotropic models of extratropical response to El Nino. *J. Atmos. Sci.* **44**, 3576–3586.

Held, I. M., S. W. Lyons and S. Nigam, 1989. Transients and the extratropical response to El Nino. *J. Atmos. Sci.* **46**, 163–174.

Holton, J. R. 1992. *An introduction to dynamic meteorology*. Academic Press Inc., 3rd edition.

Kalnay, E., M. Kanamitsu, R. Kistler, W. Collins, D. Deaver, L. Gandin, M. Iredell, S. Saha, G. White, J. Woollen, Y. Zhu, A. Leetma, R. Reynolds, M. Chelliah, W. Ebisuzaki, W. Higgins, J. Janowiak, K. C. Mo, C. Ropelewski, J. Wang and R. Jenne, 1996. The NCEP/NCAR 40-year re-analysis project. *Bull. Am. Met. Soc.*, March 1996.

Kok, C. J. and J. D. Opsteegh, 1985. On the possible causes of anomalies in seasonal mean circulation patterns during the 1982/83 El Nino event. *J. Atmos. Sci.* **42**, 677–694.

Kushnir, Y. 1994. Interdecadal variations in North Atlantic sea surface temperature and associated atmospheric conditions. *J. Climate* **7**, 141–157.

Latif, M. and T. P. Barnett, 1994. Causes of decadal variability over the North Pacific and North America. *Science* **266**, 634–637.

Lenderink, G. and R. J. Haarsma, 1994. Variability and multiple equilibria of the thermohaline circulation associated with deep water convection. *J. Phys. Oceanogr.* **24**, 1480–1493.

Lenderink, G. and R. J. Haarsma, 1996. Rapid convective transitions in the presence of sea-ice. *J. Phys. Oceanogr.* **26**, 1448–1467.

Liu, Q. and T. Opsteegh, 1995. Interannual and decadal variations of blocking activity in a Quasi-Geostrophic model. *Tellus* **47A**, 941–954.

Marshall, J. and F. Molteni, 1993. Toward a dynamic understanding of planetary-scale flow regimes. *J. Atmos. Sci.* **50**, 1792–1818.

Palmer, T. N. and Sun Zhaobo, 1985. A modelling and observational study of the relationship between sea surface temperature in the north-west Atlantic and the atmospheric general circulation. *Quart. J. R. Met. Soc.* **111**, 947–975.

Roads, J. O. 1987. Predictability in the extended range. *J. Atmos. Sci.* **44**, 3495–3527.

Robertson, A. W. 1996. Interdecadal variability over the North Pacific in a multi-century climate simulation. *Climate Dynamics* **12**, 227–241.

Saravanan, R. and James C. McWilliams, 1997. Stochasticity and spatial resonance in interdecadal climate fluctuations. *J. Climate* **10**, 2299–2320.

Semtner, A. J. 1976. A model for the thermodynamic growth of sea-ice in numerical investigations of climate. *J. of Phys. Oceanogr.* **6**, 379–389.

Von Storch, J. S. 1994. Interdecadal variability in a global coupled model. *Tellus* **46A**, 419–432.

Verbeek, J. 1997. Windstress and SST variability in the North Atlantic area; observations and five coupled GCM's in concert. *Mon. Wea. Rev.* **125**, 942–957.

Woodruff, S. D., R. J. Slutz, R. L. Jenne and P. M. Steurer, 1987. A comprehensive ocean-atmosphere dataset. *Bull. Amer. Meteor. Soc.* **68**, 1239–1250.